COMPLEX IMPEDANCE STUDIES OF OPTICALLY EXCITED STRONTIUM BARIUM NIOBATE

by

Midshipman Peter G. Brereton, Class of 2001
United States Naval Academy
Annapolis, Maryland

_____
(signature)

Certification of Advisers' Approval

Associate Professor Steven R. Montgomery
Physics Department

_____
(signature)

_____
(date)

Assistant Professor Charles A. Edmondson
Physics Department

_____
(signature)

_____
(date)

Acceptance for the Trident Scholar Committee

Professor Joyce E. Shade
Chair, Trident Scholar Committee

_____
(signature)

_____
(date)

USNA-1531-2

Form SF298 Citation Data

Report Date *("DD MON YYYY")* 07052001	Report Type N/A	Dates Covered (from... to) *("DD MON YYYY")*

Title and Subtitle Complex impedance studies optically excited strontium barium niobate	Contract or Grant Number
	Program Element Number

Authors Brereton, Peter G.	Project Number
	Task Number
	Work Unit Number

Performing Organization Name(s) and Address(es) US Naval Academy Annapolis, MD 21402	Performing Organization Number(s)
Sponsoring/Monitoring Agency Name(s) and Address(es)	Monitoring Agency Acronym
	Monitoring Agency Report Number(s)

Distribution/Availability Statement
Approved for public release, distribution unlimited

Supplementary Notes

Abstract

Subject Terms

Document Classification unclassified	Classification of SF298 unclassified
Classification of Abstract unclassified	Limitation of Abstract unlimited

Number of Pages 61	

		Form Approved **OMB No. 074-0188**

REPORT DOCUMENTATION PAGE

1. AGENCY USE ONLY (Leave blank)	2. REPORT DATE 7 May 2001	3. REPORT TYPE AND DATE COVERED

4. TITLE AND SUBTITLE Complex impedance studies optically excited strontium barium niobate	5. FUNDING NUMBERS
6. AUTHOR(S) Brereton, Peter G.	

7. PERFORMING ORGANIZATION NAME(S) AND ADDRESS(ES)	8. PERFORMING ORGANIZATION REPORT NUMBER

9. SPONSORING/MONITORING AGENCY NAME(S) AND ADDRESS(ES) US Naval Academy Annapolis, MD 21402	10. SPONSORING/MONITORING AGENCY REPORT NUMBER Trident Scholar project report no. 279 (2001)

11. SUPPLEMENTARY NOTES

12a. DISTRIBUTION/AVAILABILITY STATEMENT This document has been approved for public release; its distribution is UNLIMITED.	12b. DISTRIBUTION CODE

13. ABSTRACT:

The complex permittivity and impedance of undoped and unpoled single crystal strontium barium niobate (SBN) were measured with a computer interfaced impedance analyzer over a frequency range from 100 Mhz to 10 Khz using small AC signals with millivolt amplitudes. The thin (-2 mm) planar crystal sample was placed between the plates of a modified parallel plate capacitor and illuminated on the side with linearly polarized argon-ion laser light operating at select wavelenghts in the blue-green with photon energies that are slightly below the bandgap energy of SBN. Impedance spectra were obtained in the dark between room temperature and 70^0C and compared with impedance spectra obtained with laser illumination at room temperature. Dark measurements at all temperatures are consistent with studies in the literature that suggest electron hopping as the predominant charge transfer mechanism. Illumination markedly changed the conductivity of the crystal and the chrage transfer mechanism by elevating significant numbers of charge carriers into the conduction band. This was found to be independent of the polarization of the light and slightly dependent on its wavelength over our wavelength range of 458 nm to 515 nm. The dielectric constant of the crystal under illumination changed less than twenty per cent and is probably due to the slight heating of the crystal induced by the laser.

14. SUBJECT TERMS ferroelectric, photorefractive, electron hopping, dielectric relaxation, photoconductive			15. NUMBER OF PAGES 59
			16. PRICE CODE

17. SECURITY CLASSIFICATION OF REPORT	18. SECURITY CLASSIFICATION OF THIS PAGE	19. SECURITY CLASSIFICATION OF ABSTRACT	20. LIMITATION OF ABSTRACT

Abstract: The complex permittivity and impedance of undoped and unpoled single crystal strontium barium niobate (SBN) were measured with a computer interfaced impedance analyzer over a frequency range from 100 millihertz to 10 kilohertz using small AC signals with millivolt amplitudes. The thin (~2 mm) planar crystal sample was placed between the plates of a modified parallel plate capacitor and illuminated on the side with linearly polarized argon-ion laser light operating at select wavelengths in the blue-green with photon energies that are slightly below the bandgap energy of SBN. Impedance spectra were obtained in the dark between room temperature and 70°C and compared with impedance spectra obtained with laser illumination at room temperature. Dark measurements at all temperatures are consistent with studies in the literature that suggest electron hopping as the predominant charge transfer mechanism. Illumination markedly changed the conductivity of the crystal and the charge transfer mechanism by elevating significant numbers of charge carriers into the conduction band. This was found to be independent of the polarization of the light and slightly dependent on its wavelength over our wavelength range of 458 nm to 515 nm. The dielectric constant of the crystal under illumination changed less than twenty per cent and is probably due to the slight heating of the crystal induced by the laser.

Table of Contents

I. Introduction

Strontium barium niobate (SBN) is an optically interesting, transparent crystal. By this we mean that it both alters and is altered by visible light. This phenomenon offers several interesting and technologically important applications: as a holographic information storage medium, as a wave-guide to confine and steer beams of light, and as an amplifier and mixer of light. As a result of these optical properties, a significant amount of scientific research has been devoted to investigating the behavior of SBN. This research has firmly established that the optical nature of the crystal is a result of its conductive and dielectric properties. Very little scientific literature exists, however, on the electrical nature of SBN as it is subjected to optical stimulation. The purpose of this research is therefore to investigate the electrical characteristics of SBN under high intensity illumination.

II. Properties of SBN

For more than a quarter century, physicists and materials scientists have been studying the structure and properties of SBN. Its interesting behavior when illuminated with intense light has made SBN and other crystals with similar structure very important in optical physics with possible applications to telecommunications and laser physics.

As with all crystals, SBN is comprised of many atoms bonded together in a repeating pattern. The electrons that hold these atoms together are bound to the crystal structure. Those few electrons that are not bound to the individual atoms in the crystal lattice can move around, or conduct. Because SBN has so few of these conduction electrons, it is classified as a very good electrical insulator, called a dielectric. If a crystal

of SBN is illuminated with intense light, however, some of the non-conducting electrons can become energetically excited and mobilized to conduct through the lattice. Thus, as SBN is illuminated, it becomes more conductive to the flow of electricity.

Additionally, SBN is a special type of dielectric material known as a ferroelectric. The phenomena associated with ferroelectricity, demonstrated in detail below, lead to the extraordinary optical effects associated with SBN. To understand the photoconductive and ferroelectric nature of SBN it is necessary first to investigate the material's characteristic crystal structure and electronic configuration.

A. Structure

Strontium barium niobate is a synthesized crystal of the form $Sr_{5-x}Ba_xNb_{10}O_{30}$ and has a tetragonal tungsten-bronze structure. The unit cell for this structure, illustrated below in Fig. 2.1, consists of ten oxygen octahedra joined at the corners. Inside each octahedron resides a niobium ion. The arrangement of the niobate octahedra is such that there are several holes (called interstitial sites) in the oxygen lattice. There are five types of interstitial sites, labeled A1, A2, B1, B2, and C in Fig. 2.1. The other crystal ions reside in these sites. Barium, the largest atom in the SBN composition, will fill the largest sites, denoted A2 in the diagram. The next largest ion, strontium, is randomly distributed among remaining unfilled A2 sites and the next largest sites, labeled A1. Niobium resides in the B1 and B2 sites. The C sites in the structure are too small to accept any of the ions in SBN so remain empty for pure, undoped crystals.[1]

---

[1] M. E. Lines and A. M. Glass, <u>Principles and Applications of Ferroelectrics and Related Materials</u>, (Clarendon, Oxford, 1987), pp. 280-283.
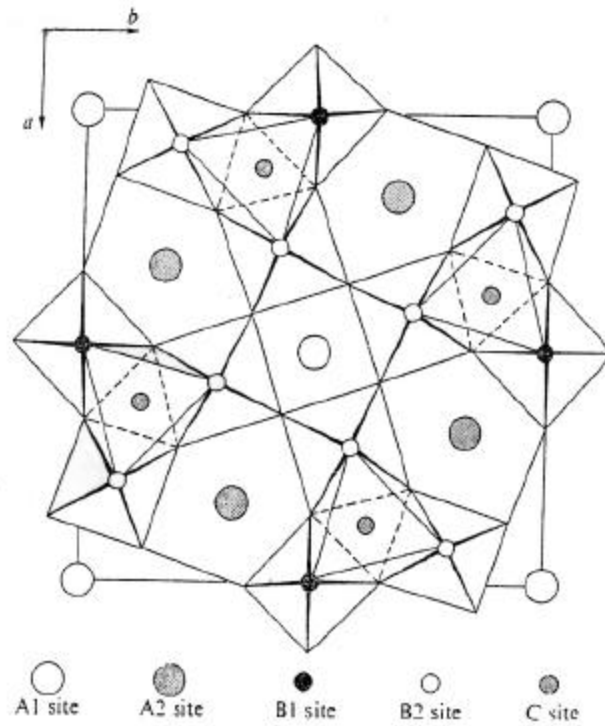
Figure 2.1: Unit cell geometry of SBN[2]. The interstitial sites are labeled A1, A2, B1, B2 and C.

B. Band Structure and Photoconductivity

While the configuration of the ions in the crystal lattice is important, it is the resulting electron distribution that gives solid-state materials, such as ferroelectric crystals, their distinct electrical properties. When a large number of atoms combine, as in a crystal lattice, their electrons interact so that only certain electron energy states can exist. The distribution of electron energy states is dominated by bands of densely packed allowed states separated by bands devoid of allowed states.

A solid-state material's electronic behavior is dictated by this distinct band structure, as illustrated below in Fig. 2.2. For insulators, the low energy band, or valence

---

[2] Lines, p. 280.

band, is completely full of electrons. The high-energy states, called the conduction

band, are empty. The energy gap between the valence and conduction bands, called the

forbidden zone or band gap, is very large. Thus, an insulator resists the flow of electrons

because there is no way for it to promote low energy electrons to the higher energy

conduction electron state: the gap is too large for many thermally excited valence

electrons to jump.

In a semiconductor, the valence band is again full and the conduction band empty

at absolute zero. However, the band gap is small enough that, at temperatures above

absolute zero, some thermally excited valence electrons will have enough energy to move

into the conduction band. This means that a small number of conducting electrons will

exist in the conduction band and will allow the flow of electricity.

A metal is a material that is a very good electric conductor. At absolute zero, the

valence band is full and the conduction band partially filled. This means that no extra

energy is needed to promote electrons into the conduction band and that electrons can
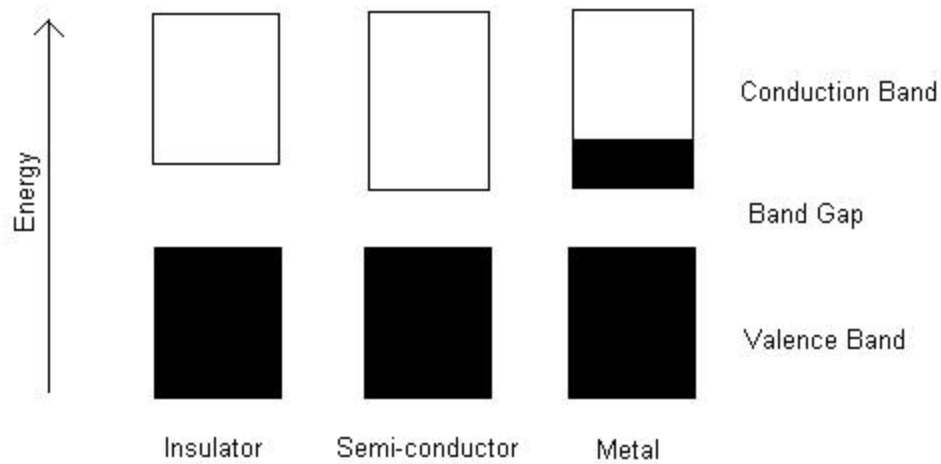
flow very easily.

Figure 2.2: Illustration of solid-state material types and energy band structure at absolute zero. The white rectangles represent empty energy state; the black show filled states.

SBN is an insulator because it has a large band gap and very few electrons in the conduction band at room temperature. Thermal excitation at normal room temperatures cannot provide very many valence electrons with sufficient energy to jump the band gap. However, light of sufficiently high frequency can promote valence electrons to the conduction band. So, under illumination, SBN becomes much more conductive. This is known as photoconductivity.

In reality, most materials classified as insulators, called dielectric materials, conduct electrons to some degree. For various reasons, there are electron energy states within the band gap. One mechanism for creating these states is the process of doping. A common example is the industrial doping of the natural semiconductor silicon. Silicon has a band gap that is narrow enough to allow a small fraction of the valence electrons to be thermally excited into the conduction band at room temperature. To increase its conductivity, silicon is often mixed, or doped, with elements from Group V of the

periodic table, such as arsenic. These atoms have one more valence electron than silicon. When added to the silicon crystal lattice, arsenic will have one unbonded electron. It exists in an energy state within the band gap, as illustrated in Fig. 2.3. Such band gap electrons require less thermal energy to be excited into the conduction band. For SBN, defects in the crystal lattice created during manufacturing and the fact that the strontium and barium ions randomly occupy interstitial sites between adjacent unit cells create many of these inter-band gap energy states.[3]
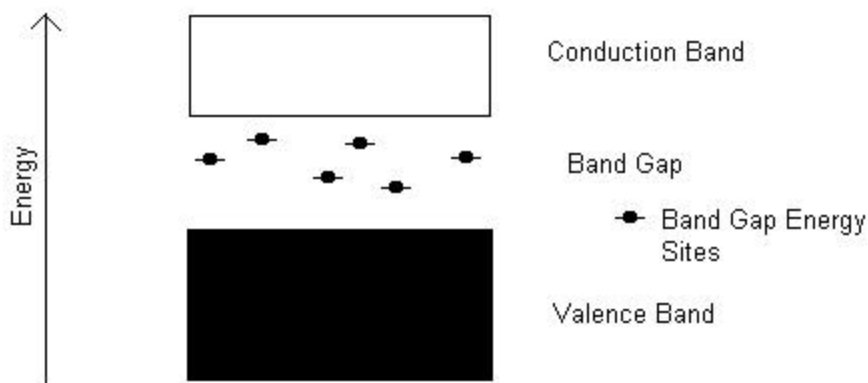
Figure 2.3: Band gap electron energy sites.

C. Ferroelectricity

One reason that SBN is such a common candidate for study is that it conveniently exhibits a property known as ferroelectricity at room temperature. Like all electrical insulators, SBN can be polarized. For a polarizable material, the positive and negative charges that make up a dielectric will separate in the presence of an electric field, creating a dipole moment (a positive and negative charge separated by a small distance). These

[3] C. Kittel, Introduction to Solid State Physics, (Wiley, New York, 1986), pp. 158-167.

dipoles will realign themselves so that the more positive end points in the direction of the applied electric field. In common dielectrics, the dipole moments will collapse and randomly rearrange themselves so that no polarization remains after the electric field is turned off. In a ferroelectric, the polarization exists even after the field is removed.[4]

At room temperature, the actual structure of SBN differs slightly from the structure introduced in Fig. 2.1. If one were able to look at SBN along the oxygen plane (i.e. looking down the *a* or *b* axes) one would see that the strontium, barium and niobium ions reside slightly above or below the oxygen plane. It is this separation of ions that gives rise to the ferroelectric nature of SBN. The dipole moments created by this separation of ions remain regardless of the applied field.

However, when that same crystal is heated above a certain temperature, known as the Curie temperature, these ions fall into the oxygen plane. This Curie temperature, T_c, is characteristic of all ferroelectric materials. It is the temperature above which there is no spontaneous polarization.[5]

At temperatures greater than T_c, SBN is in a state known as paraelectric where there is no net polarization in the absence of an applied field. The crystal lattice shifts slightly to allow the barium and strontium ions to fall into the oxygen plane. The net result is an unpolarized crystal because all positive charges reside in the same plane as the negative charge. Below T_c, the lattice contracts, pushing the positive ions out of the plane, creating the requisite charge separation. This ferroelectric mechanism of moving lattice ions is known as a displacive phase transition. The Curie temperature for SBN is

---

[4] Kittel, pp. 373-374.

[5] P. B. Jamieson, et al, "Ferroelectric Tungsten Bronze-Type Crystal Structures. I. Barium Strontium Niobate $Ba_{0.27}Sr_{0.75}Nb_2O_{5.78}$," The Journal of Chemical Physics **48**, 11 (1968).

approximately 343 K, therefore this experiment will be conducted well within the
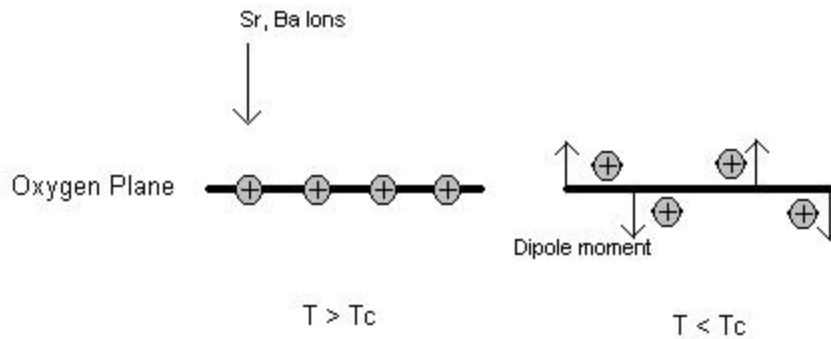
ferroelectric domain.[6]

Figure 2.5: Displacive ferroelectric transition. At temperatures lower than the Curie temperature, lattice ions are pushed out of the oxygen plane. The charge separation between the positive ions and the negative oxygen plane create dipole moments.

For a normal ferroelectric, the spontaneous dipole moments are generated

randomly, with some pointing up and some down. Through a process known as

ferroelectric poling, a crystal can be made to contain dipole moments pointing in the

same direction. A poled crystal is created by heating the ferroelectric to above T_c and

cooling it to room temperature while in a strong electric field. As the crystal cools and

the displacive phase transition moves the ions out of the oxygen plane, the external

electric field tends to force the positive ions to one side of the negative oxygen plane.

This creates many parallel dipole moments in the crystal, giving the crystal a large net

polarization.

---

[6] Kittel, p. 378

D. Optical Effects and Other Phenomena

The structure and ferroelectric nature of SBN give rise to its unique optical properties. Through a special consequence of the crystal's asymmetry and ferroelectricity, a phenomenon known as the linear electro-optic effect will cause the charge released through photoconductivity to change SBN's index of refraction to light. This change in refractive index has made it possible to store holograms in SBN, and other materials, via the photorefractive effect. In another consequence of the structural asymmetry of SBN, an applied stress will produce an electric field within the crystal, a phenomenon called piezoelectricity.

While not the primary focus of this investigation, these phenomena and the other interesting properties of SBN make it important both to research and to applications in technology. A discussion of these effects is contained in Appendix A.

III. Impedance Spectroscopy

Impedance spectroscopy is a tool used to examine the electrical properties of dielectric materials. A dielectric material is modeled as an electric circuit and the ideal circuit elements in this model represent the electrical behavior of the solid-state material.

A. Circuit Model

A capacitor is a device that stores charge and electrical energy. Capacitance, C, is the ratio of the charge on the device to the applied voltage. Potential energy is stored in

an electric field that is set up by the accumulation of charges. A simple capacitor

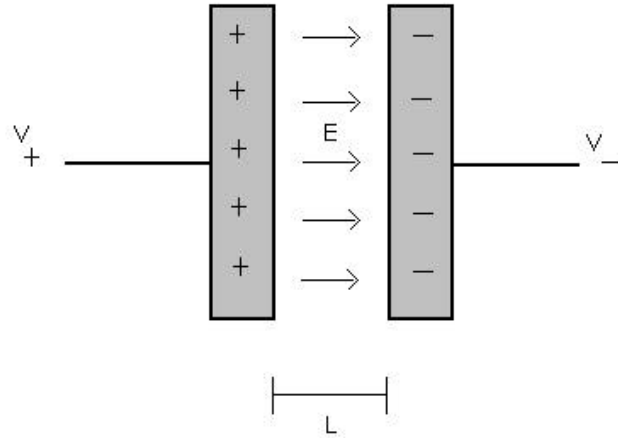model is the parallel-plate capacitor illustrated in Fig. 3.1 below.

Figure 3.1: Parallel plate capacitor with plate area, A, plate separation, L. The charge buildup set up by the applied voltage, V, creates an electric field, E.

When a voltage is applied to these parallel plates, positive charge piles up on the

plate on the left. This positive charge attracts negative charge on the right-hand plate,

creating an electric field between the plates. If there is no material between the plates,

the capacitance of this arrangement is:

$$C_0 = \frac{e_0 A}{L} \qquad\qquad (3\text{-}1)$$

where this "empty cell" capacitance is determined by the area of the plates, A; the

distance, l, between them; and the permittivity of free space, ε_0, a physical constant.

Since SBN and, indeed, all dielectric materials exhibit properties of resistance and

capacitance, the circuit model used in this experiment, shown below in Fig. 3.2, has a

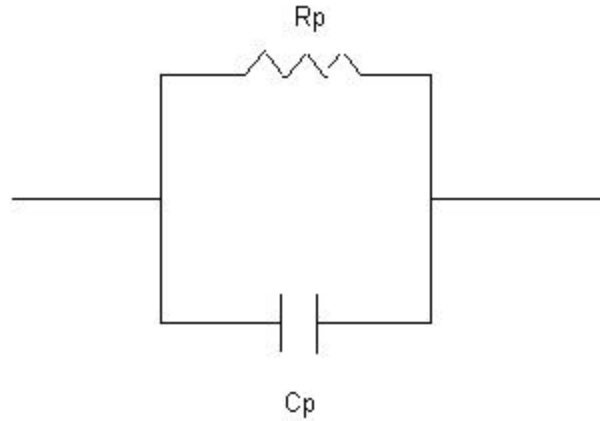parallel combination of capacitance and resistance.

Figure 3.2: Circuit model of solid-state crystal used in impedance analysis.

where R_p and C_p represent the bulk resistance and capacitance of the dielectric sample.[7]

The model in Fig. 3.2 assumes that the dielectric we are studying is a Debye dielectric. A Debye dielectric has only one distinct relaxation time or time constant defined as $\tau \equiv R_p C_p$.[8]

B. Circuit Analysis

The analysis of the circuit model in Fig. 3.2 begins by applying a sinusoidal a.c. voltage signal, V(t). It is customary to write this sinusoidal signal as:

$$V(t) = V_0 e^{iwt} \tag{3-2}$$

For this signal, V_0 is the amplitude of the voltage, and ω is its angular frequency ($\omega = 2\pi f$, where f is the frequency in Hz). It can be demonstrated that a signal in this form is

---

[7] J. R. Macdonald, Impedance Spectroscopy: Emphasizing Solid Materials and Systems, (Wiley, New York), pp. 12-16.

[8] V. V. Daniel, Dielectric Relaxation, (Academic, London, 1967), pp. 15-18.

sinusoidal by a mathematical identity called Euler's formula, that states

$e^{\pm iq} = \cos(q) \pm i \sin(q)$, where i is the imaginary number, $\sqrt{-1}$.

A voltage placed across this circuit will create a current, I(t), that is slightly out of phase with the voltage. As the capacitor is first charging up, current flows very easily, as there is no charge on the capacitor plates and there is correspondingly no voltage across the plates. As charge increases, the voltage across the plates increases and opposes current flow in the circuit. Therefore, current will always rise to its peak value before voltage in an a.c. circuit. This phase relationship is most easily represented in the following notation:

$$I(t) = I_0 e^{i(wt+f)} \tag{3-3}$$

where I_0 is the amplitude of the current, ω is the angular frequency of the voltage signal, and ϕ is the phase lead.

By Ohm's Law, the voltage and current signals for the circuit in Fig. 3.2 give the complex impedance of the circuit, a measure of the total resistance to current flow. This impedance, Z^*, is given by:

$$Z^* = \frac{V(t)}{I(t)} = \frac{V_0 e^{iwt}}{I_0 e^{i(wt+f)}} = Z_0 e^{-if} \tag{3-4}$$

The expression in Eq. 3-4 is cumbersome and hard to deal with experimentally. It is possible, through calculating the current through each circuit element, to find an expression for the impedance in terms of bulk resistance, capacitance and frequency.

The total current flowing in the circuit will split, as illustrated below, and two separate currents will flow through the resistor and the capacitor:
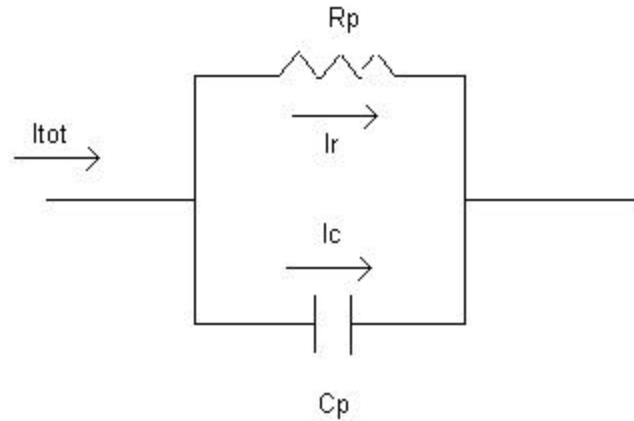
Figure 3.3: Circuit model with branch currents

Because total charge in the circuit must be conserved, we see that the total current

can be written:

$$I_{tot}(t) = I_r(t) + I_c(t) \qquad (3\text{-}5)$$

Applying Ohm's Law and the fact that that the current through a capacitor equals the

capacitance times the time rate of change of the voltage across the capacitor, Eq. 3-5

becomes:

$$\frac{V(t)}{Z^*} = \frac{V(t)}{R_p} + C_p \frac{\partial V(t)}{\partial t} \qquad (3\text{-}6)$$

Combining Eq. 3-6 and the expression for V(t), we find:

$$\frac{1}{Z^*} = \frac{1}{R_p} + i\boldsymbol{w}C_p \qquad (3\text{-}7)$$

Solving for Z^*,

$$Z^* = \frac{R_p}{1 + i\boldsymbol{w}R_p C_p} \qquad (3\text{-}8)$$

Thus, measuring the complex impedance of a dielectric material at a certain frequency will reveal information about the dielectric's bulk resistance and capacitance.[9]

C. Impedance Arc

It is customary to think of the complex impedance given in Eq. 3-8 as consisting of a real part and an imaginary part. That is, the complex impedance can be written:

$$Z^* = Z' - iZ''$$ (3-9)

where Z' is known as the real component and Z'' is the imaginary component of Z^*.

Expressions for Z' and Z'' in terms of only R_p, C_p, and ω can be found by multiplying the numerator and denominator of Eq. 3-8 by the complex conjugate of the denominator:

$$Z^* = \frac{R_p}{1 + i\omega R_p C_p} \frac{(1 - i\omega R_p C_p)}{(1 - i\omega R_p C_p)} = \frac{R_p}{1 + \omega^2 R_p^2 C_p^2} - i \frac{\omega R_p^2 C_p}{1 + \omega^2 R_p^2 C_p^2}$$ (3-10)

Comparing Eqns. 3-9 and 3-10, it is obvious that:

$$Z' = \frac{R_p}{1 + \omega^2 R_p^2 C_p^2}$$ (3-11)

and,

$$Z'' = \frac{\omega R_p^2 C_p}{1 + \omega^2 R_p^2 C_p^2}$$ (3-12)

The expressions in Eqs. 3-11 and 3-12 can be written in the following form:

$$\left[Z' - \frac{R_p}{2} \right]^2 + \left[Z'' \right]^2 = \frac{R_p^2}{4}$$ (3-13)

---

[9] Macdonald, p. 12.

A plot of Eq. 3-13, with values for Z' on the horizontal axis and Z'' on the

vertical axis will yield a semi-circle of radius $R_p/2$ centered at $Z' = R_p/2$ and $Z'' = 0$. This

is referred to as the impedance arc of the dielectric material. Our application of

impedance spectroscopy will focus on measuring and analyzing these arcs for specific

materials.

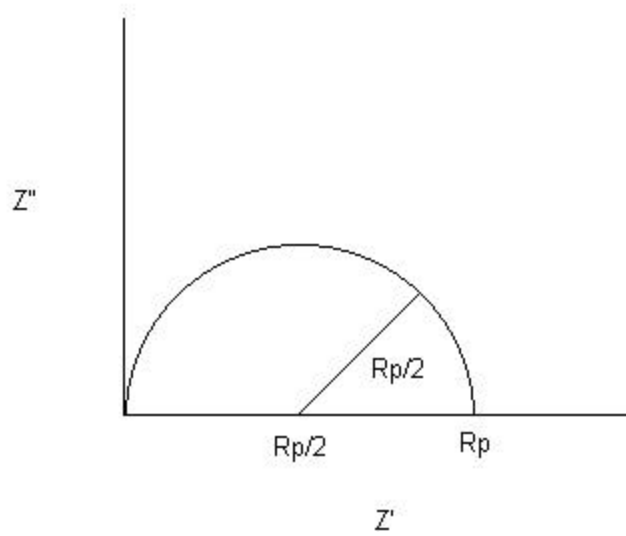*Figure 3.4: Simple impedance arc. Note that the Z' intercept is at Z' = R$_p$.*

D. The Loss Tangent

The power loss, a measure of the energy absorbed by the crystal when a voltage is

placed across it, depends on the phase lead between the voltage and current. This can be

determined by measuring Z' and Z''.

The expression for electrical power is:

$$P(t) = V_{real}(t) I_{real}(t) \qquad\qquad (3\text{-}14)$$

where V_{real} (t) and I_{real} (t) can be found from Eqs. 3-2 and 3-3 and an

examination of Euler's formula:

$$V_{real}(t) = V_0 \cos(\boldsymbol{w}t) \tag{3-15}$$

$$I_{real}(t) = I_0 \cos(\boldsymbol{w}t + \boldsymbol{f}) \tag{3-16}$$

where, by Ohm's Law, $I_0 = \dfrac{V_0}{Z_0}$.

Applying the trigonometric identity that $\cos(a+b) = \cos(a)\cos(b) - \sin(a)\sin(b)$

to the current:

$$I_{real}(t) = \frac{V_0}{Z_0}\left[\cos(\boldsymbol{w}t)\cos\boldsymbol{f} - \sin(\boldsymbol{w}t)\sin\boldsymbol{f}\right] \tag{3-17}$$

Multiplying Eqs. 3-15 and 3-17 together to find power yields:

$$P(t) = \frac{V_0^2}{Z_0}\left[\cos\boldsymbol{f}\cos^2(\boldsymbol{w}t) - \sin\boldsymbol{f}\cos(\boldsymbol{w}t)\sin(\boldsymbol{w}t)\right] \tag{3-18}$$

The expression in Eq. 3-18 gives a value for instantaneous power loss at some

specific time, t. When power loss is measured in the laboratory, only average loss over

an entire sinusoidal period is useful. The average value of a periodic function is the sum

of every value of that function over one period divided by the period. Application of this

definition yields the average power:

$$P_{av} = \frac{\int_{t=o}^{T} P(t)dt}{T}$$

$$= \frac{V_0^2}{Z_0}\cos\boldsymbol{f}\frac{\int_{t=0}^{T}\cos^2(\boldsymbol{w}t)dt}{T} - \frac{V_0^2}{Z_0}\sin\boldsymbol{f}\frac{\int_{t=0}^{T}\sin(\boldsymbol{w}t)\cos(\boldsymbol{w}t)dt}{T} \tag{3-19}$$

where T is the period for one cycle of the sinusoidal function P(t). Evaluation of

the integrals yields:

$$P_{av} = \frac{V_0^2}{2Z_0} \cos \pmb{f} \tag{3-20}$$

Custom and mathematical necessity dictate that the phase angle, ϕ, be replaced

with the complementary angle δ, where $\delta + \phi = \pi/2$. This changes Eq. 3-20 to:

$$P_{av} = \frac{V_0^2}{2Z_0} \sin \pmb{d} \tag{3-21}$$

When the angle in Eq. 3-21 is very small, $\sin \delta \cong \tan \delta$, so we find that the power

loss is proportional to $\tan \delta$, known as the loss tangent:

$$P_{av} = \frac{V_0^2}{2Z_0} \tan \pmb{d} \tag{3-22}$$

The loss tangent is related to the real and imaginary components of the complex

impedance. Applying Euler's formula to the expression for Z^* found in Eq. 3-4, the

complex impedance can be written:

$$Z^* = Z_0 e^{-if} = Z_0 \cos \pmb{f} - iZ_0 \sin \pmb{f} \tag{3-23}$$

Comparing this with $Z^* = Z' - iZ''$, the components of the complex impedance become:

$$Z' = Z_0 \cos \pmb{f} \tag{3-24}$$

and,

$$Z'' = Z_0 \sin \pmb{f} \tag{3-25}$$

Dividing Eq. 3-25 by Eq. 3-24 yields:

$$\frac{Z''}{Z'} = \tan \pmb{f} \tag{3-26}$$

From above however, it was shown that ϕ is replaced with δ, giving:

$$\tan \boldsymbol{d} = \frac{Z'}{Z''} \tag{3-27}$$

Replacing Z' and Z'' by the expressions in Eqs. 3-11 and 3-12,

$$\tan \boldsymbol{d} = \frac{1}{\boldsymbol{w} R_p C_p} \tag{3-28}$$

Therefore, the loss tangent can be determined solely from the complex impedance

and the bulk electrical properties of the material. Thus, a simple impedance measurement

can yield the power absorption of the dielectric material being investigated. Changes in

the loss tangent indicate changes in a material's crystal structure and its dielectric

behavior.[10]

E. Permittivity

The polarization of a dielectric material depends on the net dipole moment in a

volume of that material. The polarization for a linear dielectric (which SBN can be

approximated to be) depends linearly on the applied electric field:

$$\vec{P} = \boldsymbol{e}_0 \boldsymbol{c} \vec{E} \tag{3-29}$$

where the susceptibility of the material, χ, is dependent on the crystal structure of

the dielectric material.

In order to separate the applied electric field from the small fields set up by the

dipole polarization, we write the polarization and electric field in a combined relationship

called the electric displacement:

---

[10] Macdonald, p. 7.

$$\vec{D} = \pmb{e}_0 \vec{E} + \vec{P} \tag{3-30}$$

replacing the polarization with Eq. 3-29 yields:

$$\vec{D} = \pmb{e}_0 (1 + \pmb{c}) \vec{E} = \pmb{k}\vec{E} \tag{3-31}$$

where $\kappa = \varepsilon_0(1+\chi)$.

Relative permittivity, ε, also called the dielectric constant is κ divided by ε_0.

$$\pmb{e} \equiv \frac{\pmb{k}}{\pmb{e}_0} = (1 + \pmb{c}) \tag{3-32}$$

Values of the dielectric constant for many materials are found in common

resource manuals. By definition, the relative permittivity of a vacuum is 1. For

comparison, the dielectric constant of distilled water, a highly polarizable material, is

80.1.[11]

To illustrate the affects of the dielectric constant on polarization and other

electrical properties, consider the empty cell capacitor in Fig. 3.3. If a slab of a dielectric

with a characteristic dielectric constant ε and thickness l is placed between the plates, the

capacitance becomes:

$$C = \pmb{e}\frac{\pmb{e}_0 A}{l} = \pmb{e}C_0 \tag{3-33}$$

Therefore, the relative permittivity of a dielectric material tends to increase its

capacitance. This is due to the internal electric fields set up inside the dielectric through

the polarization effects of the field between the capacitor plates.

---

[11] D. J. Griffiths, <u>Introduction to Electrodynamics</u>, 3rd ed., (Prentice, New Jersey, 1999), pp. 179-180.

F. Complex Representation

Just as impedance can be written in terms of real and imaginary components, relative permittivity can be considered a complex quantity. It can be written with the usual notation as:

$$\boldsymbol{e}^* = \boldsymbol{e}' - i\boldsymbol{e}'' \tag{3-34}$$

The components of the complex permittivity can be written in terms of the bulk resistive and capacitive elements in the model circuit in Fig. 3.2. First, we must assume that the dielectric that is being modeled by this circuit has been placed in an empty cell capacitor with capacitance C_0 as described above. Then, we define the following functions, called immittance functions:

The admittance,

$$Y^* = \frac{1}{Z^*} \tag{3-35}$$

The modulus,

$$M^* = i\boldsymbol{w}C_0 Z^* \tag{3-36}$$

The admittance can be written as:

$$Y^* = G_p + i\boldsymbol{w}C_p \tag{3-37}$$

where $G_p = \dfrac{1}{R_p}$, is known as the conductance.

The complex dielectric constant can be determined from these immittances as:

$$\boldsymbol{e}^* = \frac{1}{M^*} \tag{3-38}$$

Combining this definition and Eqs. 3-36, 3-37 and 3-38,

$$\boldsymbol{e}^* = \frac{Y^*}{i\boldsymbol{w}C_0} = \frac{G_p + i\boldsymbol{w}C_p}{i\boldsymbol{w}C_0} \qquad (3\text{-}39)$$

Simplifying this expression and putting it into complex and real component form, we can determine the complex dielectric constant in terms of the bulk capacitance and resistance of the dielectric material:

$$\boldsymbol{e}' = \frac{C_p}{C_0} \qquad (3\text{-}40)$$

and,

$$\boldsymbol{e}'' = \frac{G_p}{\boldsymbol{w}C_0} \qquad (3\text{-}41)$$

Thus, Eqs. 3-40 and 3-41 depend separately on the bulk electrical components of Fig. 3.2, unlike the coupled equations for the complex impedance given in Eqs. 3-11 and 3-12. Thus, speaking in terms of the complex dielectric constant will allow us to separate conductance and capacitance changes during this experiment.

To put the complex dielectric constant in terms of the real and imaginary components of the complex impedance, Eq. 3-39 is written:

$$\boldsymbol{e}^* = \frac{1}{i\boldsymbol{w}C_0 Z^*} = \frac{1}{i\boldsymbol{w}C_0 (Z' - iZ'')} \qquad (3\text{-}42)$$

Multiplying numerator and denominator of Eq. 3-42 by the complex conjugate of Z^* leaves:

$$\boldsymbol{e}^* = \frac{Z' + iZ''}{i\boldsymbol{w}C_0 (Z'^2 + Z''^2)} \qquad (3\text{-}43)$$

Simplifying this and substituting Z_0^2 for $Z'^2 + Z''^2$ gives:

$$e' = \frac{Z''}{wC_0 Z_0^2} \tag{3-44}$$

and,

$$e'' = \frac{Z'}{wC_0 Z_0^2} \tag{3-45}$$

G. Impedance Bridge

Complex impedance is measured with a sensitive device known as an impedance

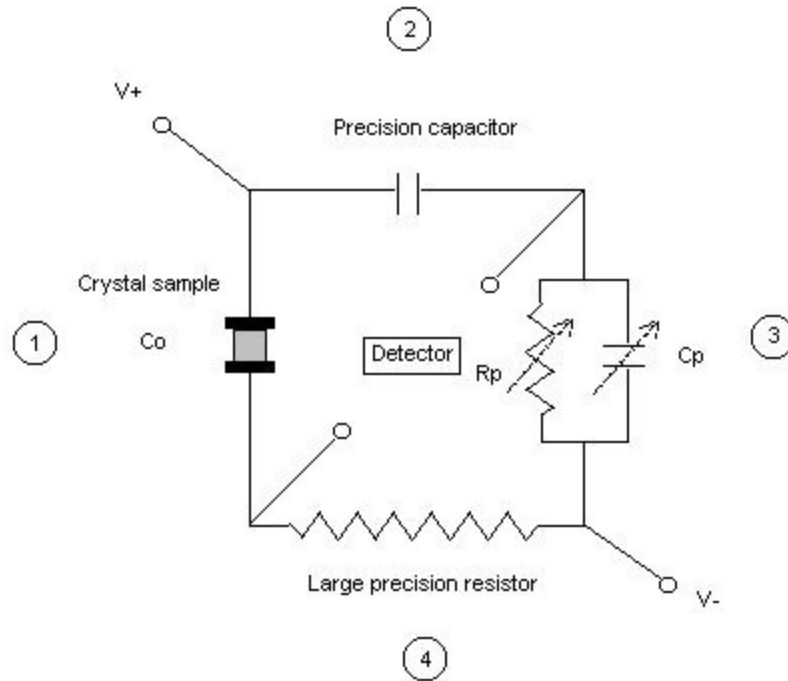bridge. A very simple impedance bridge is illustrated below in Fig. 3.5:

Figure 3.5: Simple impedance bridge[12]. A known voltage, V, is applied and the R_p and C_p values adjusted until the detector measures a null voltage.

---

[12] Daniel, p. 88.

The dielectric sample is placed in the capacitor, C_0, in arm 1. Arms 2 and 4 consist of a high precision fixed capacitor and resistor. Arm 3 is the circuit given in Fig. 3.2 with variable resistance and capacitance. An alternating voltage is applied across two corners of the bridge. R_p and C_p are then tuned until a detector between the opposite corners of the rectangle detects zero voltage. The bridge is now balanced.

For a balanced bridge, the impedances of each arm are related so that:

$$Z_1^*(\boldsymbol{w})Z_3^*(\boldsymbol{w}) = Z_2^*(\boldsymbol{w})Z_4^*(\boldsymbol{w}) \tag{3-46}$$

Since Z_2^*, Z_3^*, and Z_4^* are known quantities, the impedance of the dielectric sample can be calculated easily and an arc computed.[13]

Modern industrial bridges such as the one used in this investigation are not nearly as simple as Fig. 3.5. Most measure the current and phase lag of the electrical signal through the dielectric sample and use computer programs to calculate the impedance and bulk electrical properties. Real materials will not produce the ideal impedance arcs discussed above. For instance, a non-Debye dielectric that has several time constants will produce a depressed arc (the center of the arc is located below the Z' axis). Nonetheless, the developments above lay out adequately the requisite theory and equations to analyze the impedance data produced in this investigation.[14]

---

[13] Daniel, p. 88.
[14] Macdonald, pp. 15-17.

IV. Experiment

The basis for this experiment is the assumption that illuminated SBN will be significantly more electrically conductive than the dark sample. By combining impedance spectroscopy and illumination at various optical powers and wavelengths, the mechanisms behind this change in conductivity can be explored.

A. Crystal Sample

This experiment was conducted on an unpoled crystal slab of pure SBN. The transparent single crystal, pictured below in Fig. 4.1, is a platelet 1.1 mm thick. In order to ensure good electrical contact between the sample and the impedance spectrometer, it was necessary to coat the large faces of the crystal with a conducting electrode layer. Initially, a thin layer of gold was deposited on the sample through a sputtering process. The gold did not adhere well to the crystal surface and flaked off easily. To combat this problem, the gold was removed and the crystal faces were polished with a polishing wheel. Then, the crystal was coated with an aluminum film with a vacuum evaporator. The aluminum, while not as malleable as the gold, adhered much better and provided good electrical contact.
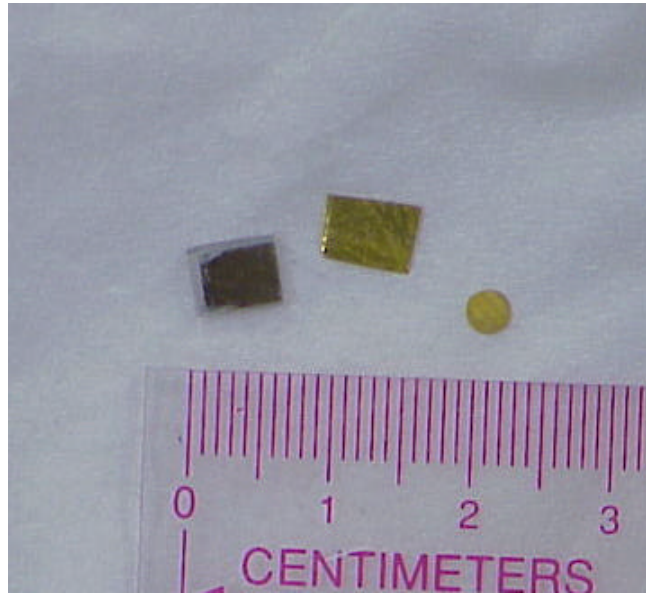
Figure 4.1: From l-r, the aluminum-coated SBN sample, the gold foil placed between the sample and the top plate of the test cell, and the gold foil placed between the sample and the center test probe.

B. Impedance Spectroscopy Setup

The impedance bridge for this experiment is a Schlumberger SI 1255 Solartron HF Frequency Response Analyzer. The bridge is interfaced with control and analysis software on an IBM PC through a General Purpose Information Bus. The Solartron impedance analyzer is capable of generating signals over a large dynamic frequency range from 10^{-6} to 10^6 Hz.

The test cell for the crystal sample is a parallel plate capacitor specially constructed to minimize fringing fields from the plate edges and provide accurate approximations of the empty cell capacitance. Seen in the schematics and photograph below, the test cell consisted of a bottom plate with an electrically isolated center probe with a diameter of 3.1 mm. When the plates are separated by 1.1 mm (the thickness of the crystal sample) the empty cell capacitance, C_0, is 0.056 pF.

The crystal sample was placed on this bottom stage with a small circle of gold foil with the same diameter as the probe to improve electrical contact between the aluminum electrodes on the crystal and the probe. The top stage was a circular plate of copper with a spring tension device to hold the crystal in place. A second sheet of gold foil was sandwiched between the top stage and the crystal sample. The signal from the Solartron analyzer was fed into coaxial cables and attached to the test cell. Because of its careful construction, the entire test cell was electrically grounded except for the bottom probe and the top plate. Because of this, fringing fields around the probe edges were kept to a minimum.
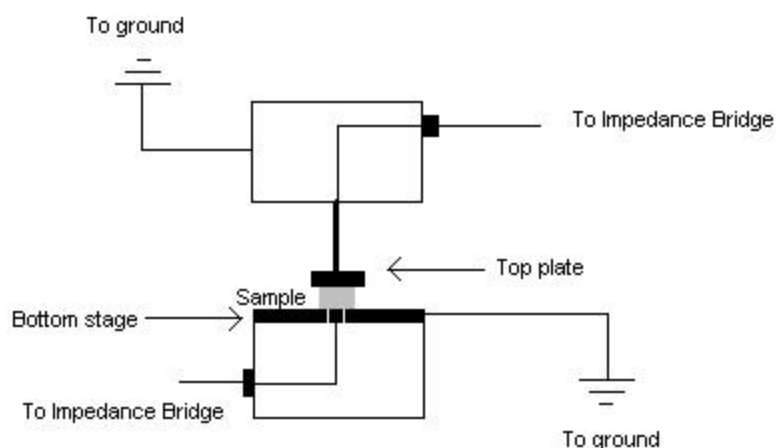

Figure 4.2: Schematic of test cell. The stage is electrically grounded except for the center probe of the bottom plate and the top electrode plate.

Bottom Stage

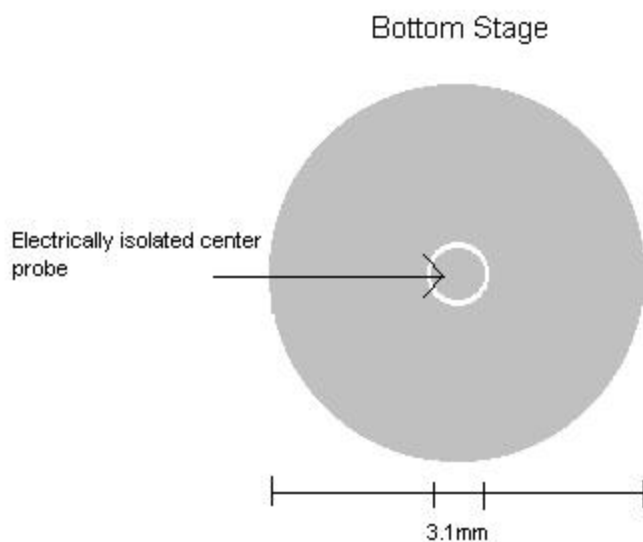Electrically isolated center
probe

3.1mm

Figure 4.3: Diagram of the bottom stage of the test cell. The stage is constructed from copper. The inner circle of 3.1 mm diameter is insulated from the rest of the stage. The sample is placed on a small circle of gold foil on the center probe. The rest of the stage is connected to ground.
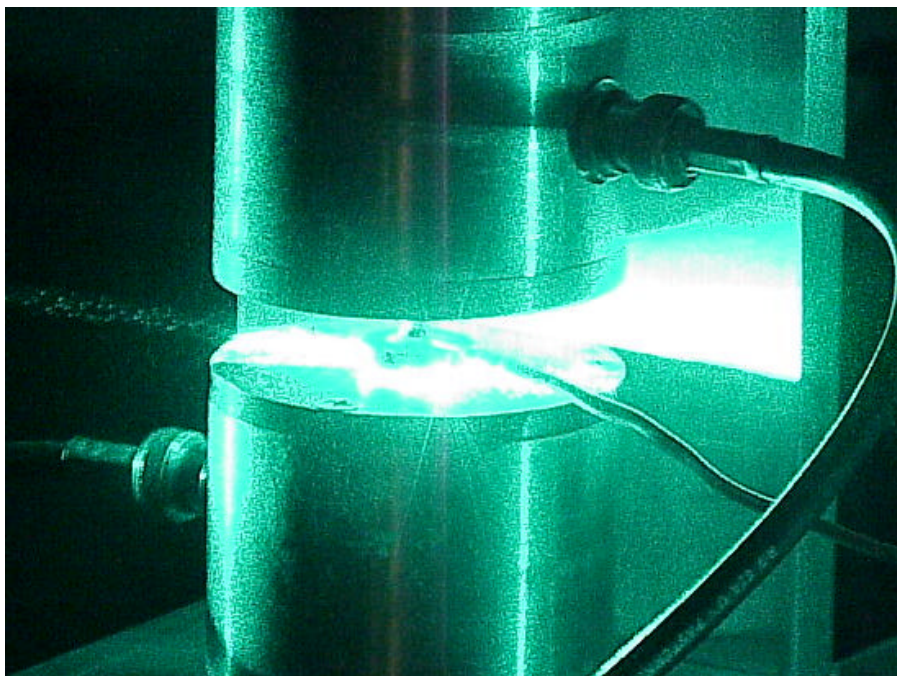

Figure 4.4: Test cell under 488nm illumination. The right hand side coaxial cable carries the low voltage signal from the Solartron impedance bridge; the left side cable carries the high voltage signal. The wire attached to the top plate of the sample holder is a thermocouple used to measure temperature

C. Optical Setup

For the purposes of this investigation, we needed to obtain a stable, powerful laser source and an optical setup that allowed us to control the intensity and polarization of the illumination that reached the crystal. The laser used was a Spectra-Physics argon-ion laser capable of outputting light at 458, 477, 488, and 515 nm at output powers up to 3 Watts.

The optical layout, as illustrated below, passed the laser output through a cylindrical lens in order to spread the beam out along the horizontal axis. The large convex lens focused this wide beam into a controllable wedge of light. By placing the test cell at different distances from the lens, we could determine exactly what volume of the crystal was being illuminated. For this experiment, we desired that the entire volume of the crystal be illuminated. The sample holder was positioned so that the beam waist at the sample was 2.59 mm, which is about twice the height of the crystal.
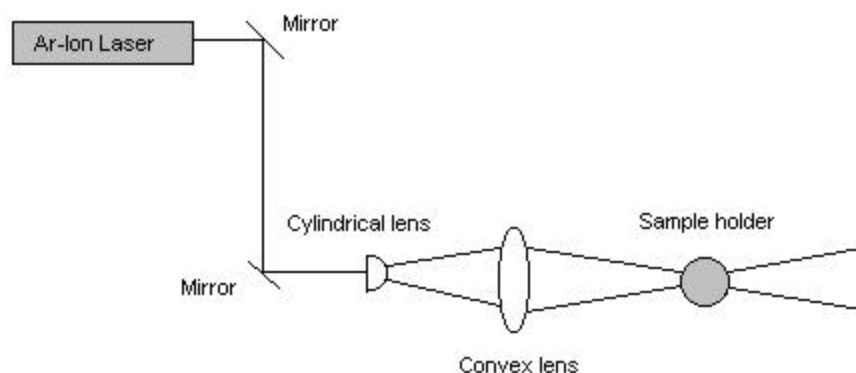

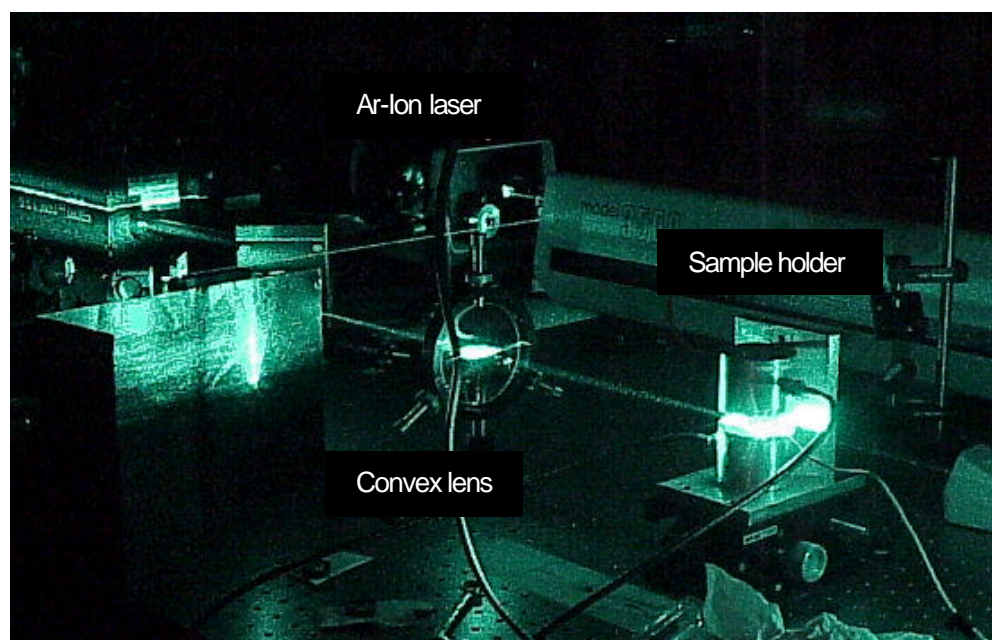
Figure 4.5: Optical table layout.

Figure 4.6: Sample illuminated with 488nm light. Shown is the large convex lens and the sample holder. The cylindrical lens is obscured by a beam trap. Note the flat wedge of light that illuminates the crystal.
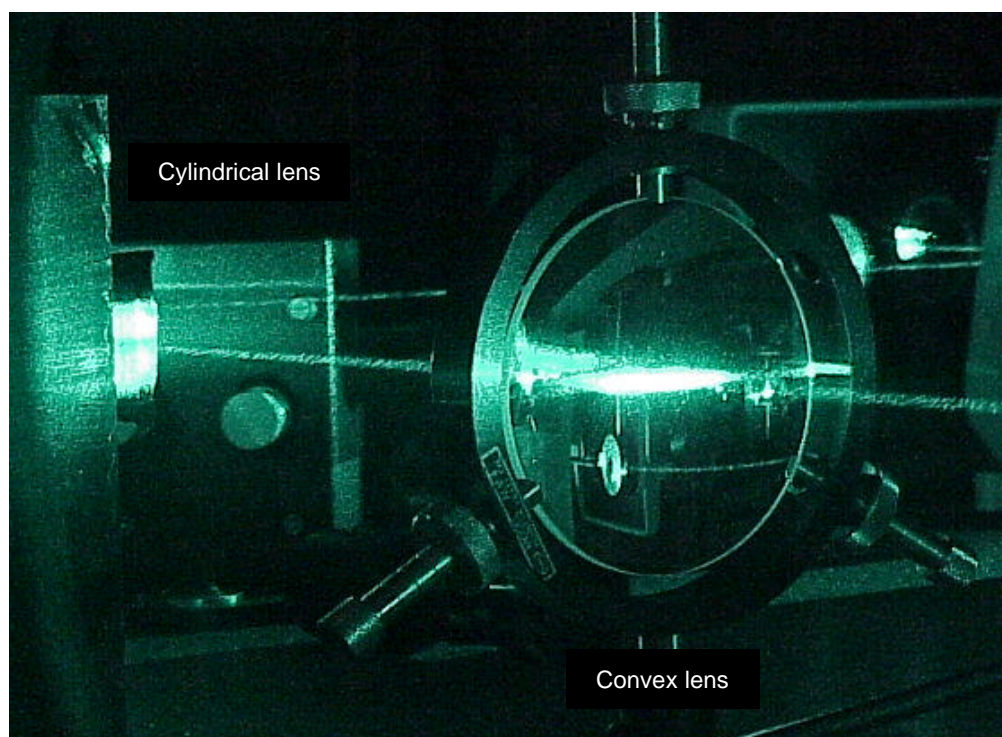

Figure 4.7: Cylindrical and convex lenses.

D. Absorption and Polarization Data

Before an optical experiment could be performed on this sample, it was necessary to determine how it affects light. Two benchmarks of a crystal's response to light are its absorption spectrum and the orientation of the c-axis.

Owing to the band structure discussed in Chapter II, solid-state materials absorb certain wavelengths of light more than others. To get the SBN absorption spectrum in the visible and ultra-violet regimes, the sample was placed in a Hewlett Packard 8452A Diode Array Spectrophotometer. This device passed light at wavelengths from about 200nm to 700nm through the sample to a detector that measured the amount of light absorbed by the sample. The resulting spectrum, shown below in Fig. 4.8, shows that the crystal is very transparent until approximately 390nm. This sharp increase in absorbance is known as the band-edge and is a measure of the band-gap energy of the crystal. Photons in 390nm or shorter wavelength light have enough energy to excite valence electrons to the conduction band.

At a range of wavelengths from 390nm to approximately 600nm, the crystal exhibits non-zero absorption. This is compelling evidence for inter-band sites. Electrons in inter-band sites need less energy to be excited into the conduction band than do the valence electrons. Therefore, the relatively low concentration of inter-band energy electrons absorbs some of the lower energy, longer wavelength light.
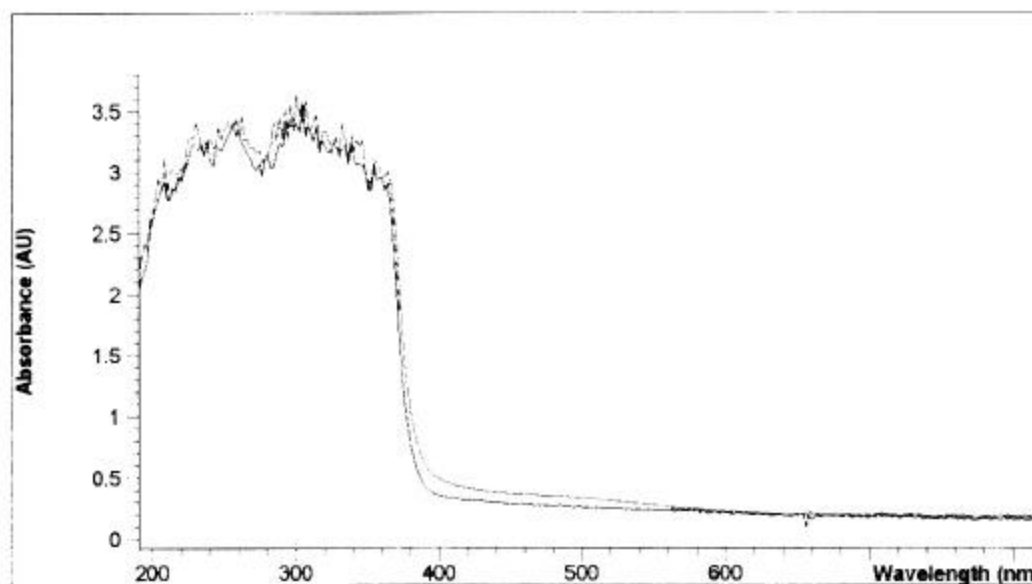
Figure 4.8: UV-Visible absorption of SBN (dashed line is the absorption of a cerium doped sample of SBN to be used in further experiments)

A similar study of absorption in the far infrared region conducted with a Bio-Rad Excalibur FTS-3500 ARX FT-IR Spectrometer revealed that the pure sample does not have any significant absorption in the longer wavelength infrared spectrum.

The Argon-Ion laser is therefore a good tool for investigating optical effects in SBN because all of its emission lines have longer wavelengths than the band-edge and are not completely absorbed by the sample. At the same time, appreciable amounts of inter-band electrons would be promoted to the conduction at the wavelengths emitted by the Argon-Ion laser.

In addition to being photoconductive and ferroelectric, SBN is also birefringent. A birefringent crystal has a different index of refraction along the c-axis (for SBN, this is the axis perpendicular to the oxygen plane, pictured in Fig. 2.1) than the other crystal axes. If the c-axis of a birefringent crystal is perpendicular to the light incident to that

crystal, light will exit the crystal with one component affected by the index of

refraction of the c-axis and another component affected by the other index.[15] To test this,

the sample was illuminated with light polarized first parallel and then perpendicular to

the sample holder plates. The exit beam was viewed through a second polarizer. If the

second polarizer could be rotated to some angle and all the light exiting the crystal was

blocked, this is evidence that the c-axis is parallel to the direction of the incident beam:

the light beam was affected by only one index of refraction. If no amount of rotation

blocks all the light, then the c-axis is perpendicular to the light beam. Using this

procedure, it was determined that the c-axis for our SBN sample was oriented in a plane

parallel to the light incident on the sample holder.

E. Experimental Procedure

Once the sample had been properly seated in the test cell and the optics

sufficiently tuned and focused, the experiment itself was quite simple. After warming up

the laser and impedance spectroscopy apparatus, the Solartron software controller was

configured to apply a signal over a specified range of frequencies across the sample

holder plates. For most measurements, the lowest frequency was either 0.1 or 1.0 Hz and

the highest 1.0 MHz. Once the dark impedance measurement was completed and stored,

the crystal was illuminated with the Argon-ion laser at 0.5 Watt output power. Table 4.8

below lists the approximate incident intensity and optical power on the crystal sample at a

given laser output power. It is interesting to note that the intensities used in this

experiment were of the same order of magnitude as those commonly used to in wave-

---

[15] G. R. Fowles, Introduction to Modern Optics, (Dover, New York, 1975), p. 169.

guide experiments on SBN. The Solartron impedance software was run again and the

illuminated measurements stored. This procedure was repeated in increments of 0.5 Watt

to a maximum of 3.0 W laser power.

Laser Power (W)	Incident Intensity (kW/m^2)	Incident Power (mW)
0.5	30	320
1.0	60	640
1.5	90	964
2.0	120	1298
2.5	150	1610
3.0	180	1930

Table 4.8: Approximate optical intensity and power incident on crystal at a given laser output power

V. Results

The experimental results presented below represent the data obtained from a

single configuration of the SBN sample in the parallel plate test cell. The uncertainties in

these measurements are quite small, on the order of a few percent. The values presented

below: conductance, capacitance, impedance, and loss tangent, are dependent on the

dimensions and configuration of the sample and test apparatus. The trends in this data,

however, are quite representative of the electrical behavior of SBN in general.

A. Impedance Plot for 488nm

A plot of the complex impedance data for SBN illuminated at 488nm at

increasing laser output power reveals the impedance arcs shown in Fig. 5.1. When

graphed as Z'' against Z', the low frequency data plots on the far right side of each

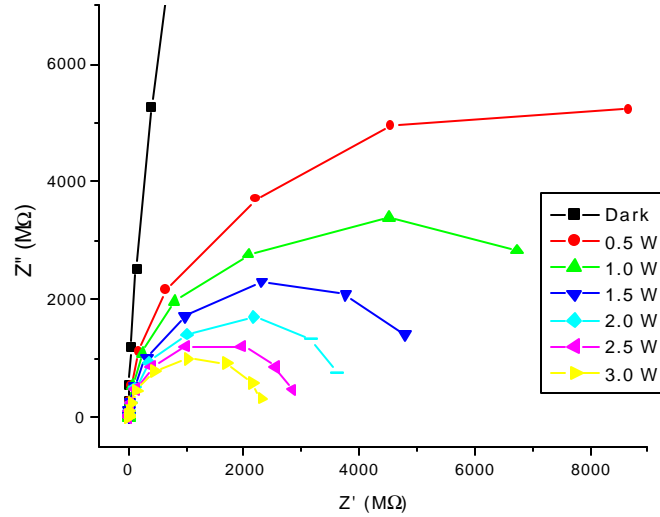curve and high frequency points fall on the left side.

Figure 5. 1: Impedance plot for SBN illuminated with 488nm at 0.5W to 3.0W laser power. The frequency of the applied voltage signal ranges from 0.1 Hz to 1.0 MHz for this data.

From Eq. 3-13, the right-most Z' intercept of the arc is at $Z' = R_p$, the bulk

resistance of the sample. The intercept for the dark sample occurs at a frequency beyond

the present experimental range, but is approximated, through several low frequency

measurements, to be on the order of 10^{12} Ω. Under illumination, the SBN becomes much

more conductive. The impedance arcs become smaller, and the Z' intercept decreases.

A close examination of the arcs themselves shows that, especially at low optical

powers, the arcs are depressed or have their centers below the Z'-axis. This depressed arc

implies that, in the dark and at low output powers, SBN tends to behave like a non-

Debeye dielectric. As power is increased however, the arc becomes more semicircular,

indicating that the crystal is closer to the ideal Debeye dielectric with a single time

constant.[16]

B. Conductance and Electron Transport Mechanism

The logarithmic plot of conductance against frequency for SBN at 488nm is given
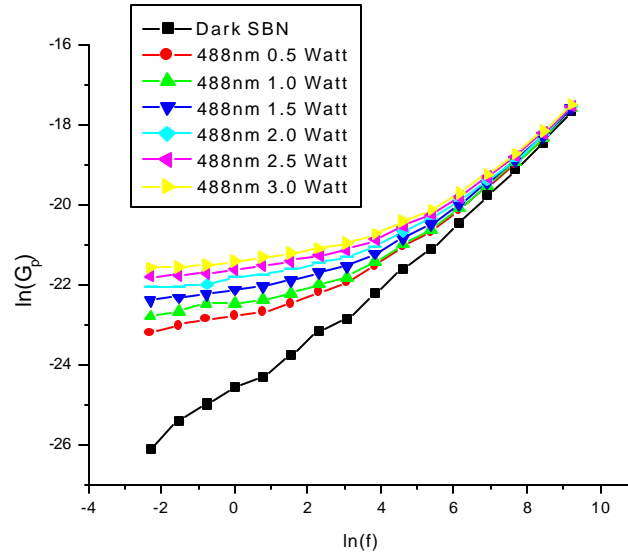
in Fig. 5.2:

Figure 5.2: Conductance, G_p vs. frequency of applied voltage for SBN at 488nm

The first significant feature of Fig. 5.2 is the approximately linear nature of the

dark conductance data. A linear slope in the log-log plot of conductance vs. frequency

means that G_p is proportional to f^s, where s is the slope of the log-log line. This implies

that the primary electron transport mechanism in dark SBN is electron hopping. Electron

---

[16] Macdonald, pp. 15-17.

hopping occurs when thermally excited electrons hop from one adjacent site to another without first being excited into the conduction band.[17,18,19]

From Fig. 5.2, it is obvious that dark SBN exhibits electron-hopping behavior. Under illumination, however, the log-log conductance curves become strongly non-linear, especially at low frequencies. This is compelling evidence that illumination changes the material's electron transport mechanism.

M. Abkowitz, et al, showed in a 1974 paper on electron hopping that hopping is the main transport mechanism for many highly insulating crystalline and amorphous photoconductive materials.

Furthermore, there is a strong qualitative agreement between the illuminated conductance of our SBN sample and the amorphous photoconductive materials investigated by Abkowitz. The same low frequency non-linearities are observed in both cases.

However, Abkowitz determined that the change in conductance, $\Delta G \equiv G_{ill} - G_{dark}$ (where G_{ill} and G_{dark} are the illuminated and dark conductance, respectively), was frequency independent. We observed that the increase in conductance for SBN does depend on the frequency of the applied electrical signal. The conductance change for SBN at 1.0, 2.0, and 3.0 W of laser power are given in Fig. 5.3:

[17] M. Pollak and T. H. Geballe, "Low-Frequency Conductivity Due to Hopping Processes in Silicon," Phys. Rev. **122**, 6 (1961)

[18] M. Pollak, "Temperature Dependence of ac Hopping Conductivity," Phys. Rev. **138**, 6A (1965)

[19] M. Pollack, "Approximations for the ac Impurity Hopping Conduction," Phys. Rev. **133**, 2A (1964)
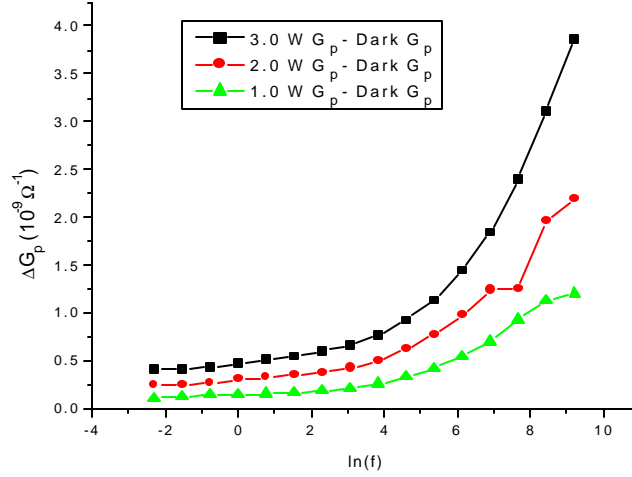
Figure 5.3: Change in conductance vs. frequency of the applied voltage. Note that the change from 10^{-2} Hz to 100 Hz is approximately independent of applied frequency while the data above 100 Hz is highly dependent.

At low frequencies, the data in Fig. 5.3 does exhibit very weak frequency dependence similar to the results noted by Abkowitz in his crystalline and amorphous insulators. Above approximately 100 Hz, however, the change in conductance in SBN becomes very dependant on frequency. While the low frequency conductance is roughly proportional to laser power, the data above 100 Hz is not. There is a disproportionately greater increase in high-frequency conductance at high laser power than at low power.[20]

The ΔG power dependence is illustrated in Fig. 5.4:

[20] M. Abkowitz, et al, "AC Conductivity and AC Photoconductivity in Amorphous and Crystalline Insulators," Phys. Rev. **9**, 4 (1974).
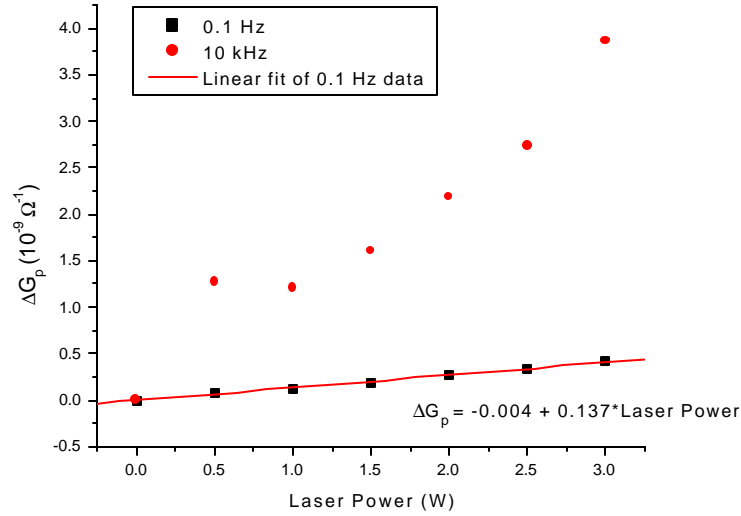
Figure 5.4: Power dependence of ΔG for 0.1 Hz and 10 kHz data.

From Fig. 5.4, we see that, at low frequencies, in this case 0.1 Hz, an increase in power yields a corresponding linear conductance response. At high frequencies, however, this linear relationship breaks down and increasing laser power yields disproportionate increases in the conductance of SBN, as shown by the nonlinear curve for the 10 kHz data.

C. Loss Tangent

The loss tangent has been shown in Chapter III to be a measure of electrical power loss. The loss tangent data for SBN under 488nm illumination is given in Fig. 5.5.
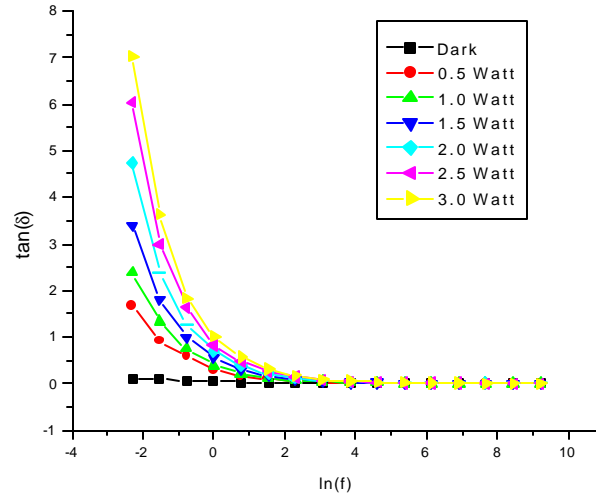
Figure 5.5: Semi-log plot of loss tangent vs. frequency of the applied voltage for 488nm

In the dark, there is very little power loss. As optical power is increased, the low

frequency power loss increases substantially. From Fig. 5.2, it is obvious that

conductance increases significantly under illumination. This increase in conductance

may account for the large spike in the sample's loss tangent. As more charge is released

through photoconductance, more of the power supplied by the applied signal can be

absorbed by the sample. Therefore, we would expect to see an increase in power loss

with the corresponding increase in conductance.

D. Temperature Dependence

Depositing up to 1900 mW of optical energy on a small crystal will tend to heat it

up through optical absorption. This thermal energy will have some effect on the

electrical properties of the crystal. It is therefore necessary to demonstrate for this

experiment that the drastic electrical changes observed are due to optical excitation and not thermal effects.

In order to determine how much the crystal's temperature was changing under illumination, a thermocouple (an electrical device that measures temperature) was put in thermal contact with the top plate of the test cell. The crystal was then illuminated with 1.0W of output power at 477, 488, and 515nm and allowed to come to thermal equilibrium. The highest temperature recorded was 24.2°C at 477nm, only about five degrees above the average room temperature.

The thermocouple was also placed in the beam behind the crystal to determine the magnitude of any other absorption temperature effects. The highest temperature measured was 32.7°C, again at 477nm. As soon as the beam was blocked, the measured temperature decreased rapidly, an indication that this heating was predominantly due mostly to the optical absorption of the dark thermocouple. This is not likely the case for the crystal.

These tests gave us a good indication of the heating magnitude: the crystal temperature would increase at most 10-12°C and most likely only 4-5°C under illumination.

Once this range was established, the test cell and SBN sample were placed in an insulating box with a variable heat source. The test cell was attached to the Solartron bridge and the thermocouple placed in contact with the sample stage. Measurements were conducted from room temperature to almost 70°C, more than twice the largest observed temperature under illumination.

The impedance data for SBN at elevated temperatures from 1.0 Hz to 1.0 MHz
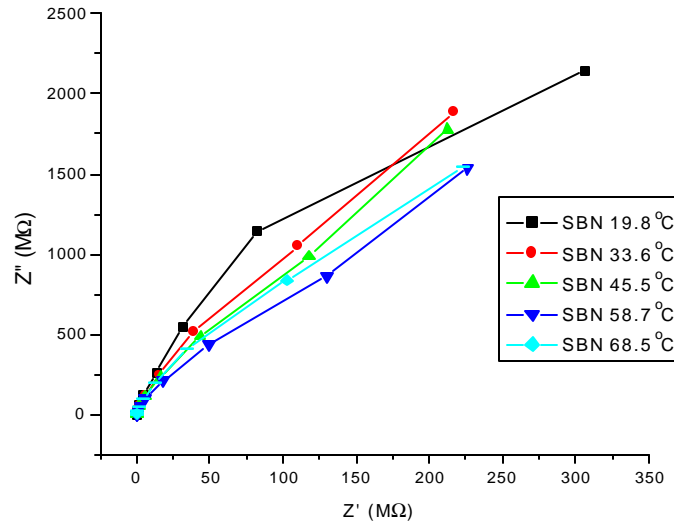
is given in Fig. 5.6:

Figure 5.6: Complex impedance of heated SBN from 1.0 Hz to 1.0 MHz applied voltage frequency.

Comparing Fig. 5.6 with the 1.0 Hz to 1.0 MHz impedance data produced under

illumination in Fig. 5.1, it is obvious that elevated temperatures do not affect the bulk

resistance of SBN with nearly the same magnitude as does optical excitation.

Even more compelling evidence that thermal effects are different from optical

changes comes from comparing the bulk capacitance and loss tangent data. Under

illumination, the capacitance of SBN did not exhibit significant changes from the dark
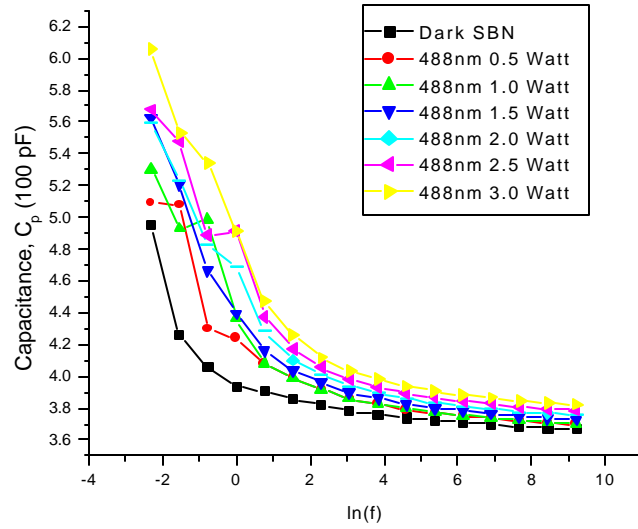
data:

Figure 5.7: Capacitance, C_p, for SBN under illumination with 488nm.

An examination of Fig. 5.7 shows that, even at low frequencies, the capacitance

values for the illuminated measurements do not vary greatly from the dark sample.

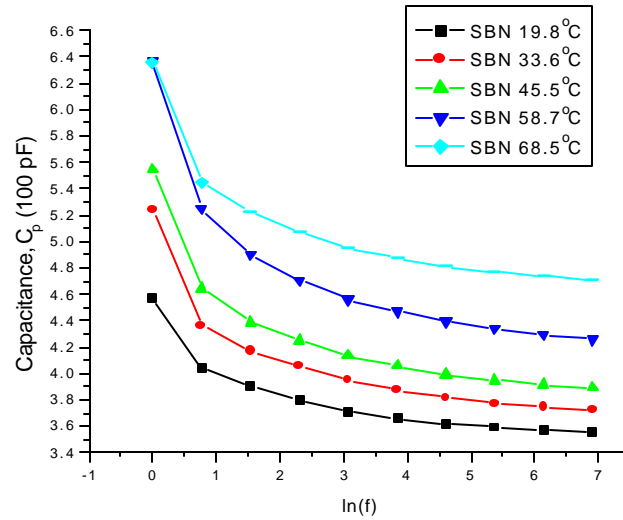With elevated temperature, however, this capacitance changed significantly:

Figure 5.8: Capacitance, C_p, for SBN at increasing temperature.

Comparing Fig. 5.8 with Fig. 5.7, it is obvious that increasing the temperature

tends to shift the capacitance of the SBN sample up uniformly over all frequency

regimes, while illumination does not.

The difference between the dark and illuminated capacitance curves in Fig. 5.7

can be used to further justify the temperature range established with the thermocouple

data. The change in capacitance at 1.0 kHz between dark SBN and the sample

illuminated with 3.0 W of 488nm light is 16.6 pF from Fig. 5.7. Correspondingly, a

capacitance increase of 16 pF in Fig. 5.8 coincides with a temperature change of 14°C.

The final evidence that the changes observed at 488nm were not due to optical

heating of the crystal comes from the loss tangent and conductance data. Fig. 5.4 shows

a substantial increase in the low frequency power loss under illumination. Under a

temperature increase, however, the loss tangent shown in Fig. 5.9 varies only slightly
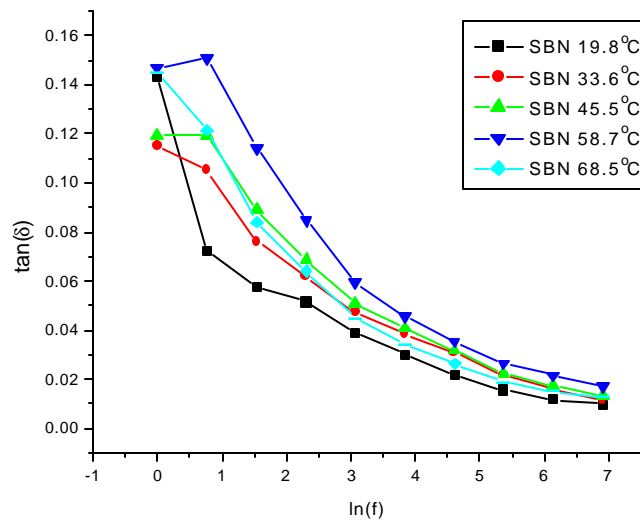
from the room temperature sample.

Figure 5.9: Semi-logarithm plot of the loss tangent vs. applied voltage frequency for temperature data.

Fig. 5.2, the log-log plot of conductance versus frequency for various laser powers, showed that the electron transport mechanism changes between the dark and illuminated measurements. The same plot for various temperatures, given in Fig. 5.10, exhibits none of the strong non-linearities observed under illumination.
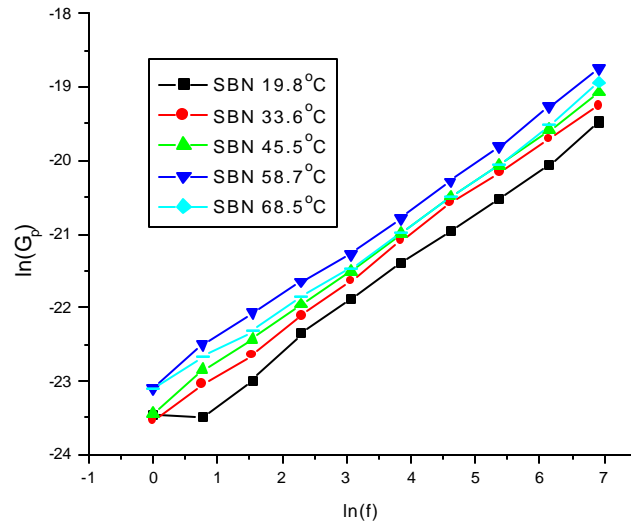
Figure 5.10: Logarithm plot of conductance, G_p vs. frequency for elevated temperature.

Even at an increase of 50°C above room temperature, the conductance plot for SBN is strongly linear. Obviously, the optical data shows a very strong non-linear deviation that is absent in the temperature data. Thus, the small temperature increase that occurs under illumination cannot be the cause of the striking changes seen in Fig. 5.2. The conduction mechanism for dark SBN appears to remain electron hopping from room temperature to 70°C. Photoconductivity, and not thermal effects must then dominate the changes observed in the optically stimulated conductance measurements. These results

confirm that the electrical changes recorded in Sections A, B and C are dominated by optical excitation.

E. Wavelength and Polarization Effects

The optical set-up for this experiment is flexible enough to support investigations across a spectrum of wavelengths and polarizations. Looking at the impedance data in Fig. 5.10 at 458, 488, and 515nm reveals that the observed changes are stronger for shorter wavelengths. This was expected, as shorter wavelength light has more energetic photons and could therefore excite more band-gap electrons to the conduction band.
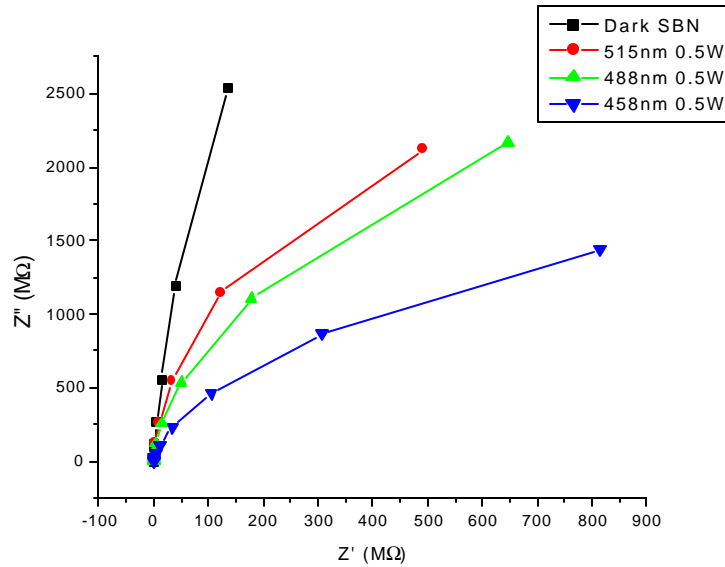

Figure 5.11: Impedance plot for 1.0 Hz to 1.0 MHz frequency of the applied voltage for SBN at 0.5 W laser light at 458nm, 488nm, and 515nm.

Similar trends are obvious in the conductance data, shown in Fig. 5.12:
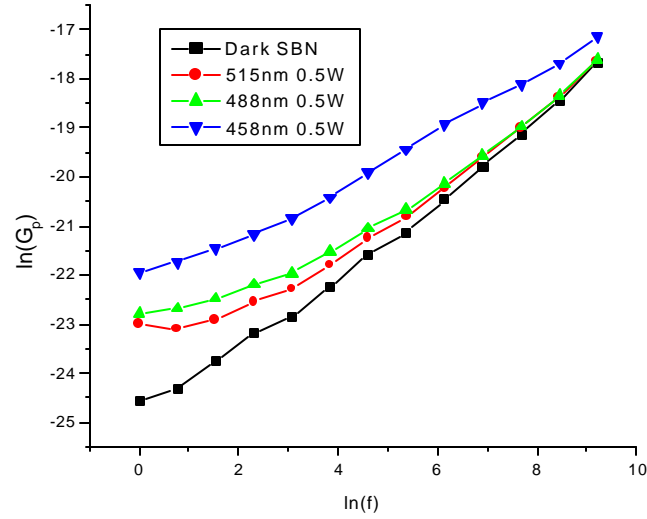
Figure 5.12: Log plot of conductance vs. frequency of the applied voltage at 515, 488, and 458nm.

The most substantial change in electron transport is found at the shortest, most energetic optical wavelength.

Polarization of light refers to the orientation of the electric field component of electromagnetic waves that make up the radiation. The direction of the polarization indicates the plane in which the electric field vector of the light wave oscillates. Using a tunable polarizer between the laser and the cylindrical lens, we illuminated the crystal with horizontally and vertically polarized 515nm light at 0.5W. The results are summarized below in Figs. 5.13 and 5.14.

Figure 5.13: Impedance plot at 0.1 Hz to 1.0 MHz frequency of the applied voltage for SBN illuminated

with unpolarized and polarized 515nm light at 0.5W

Figure 5.14: Log plot of conductance vs. frequency of the applied voltage for polarized light.
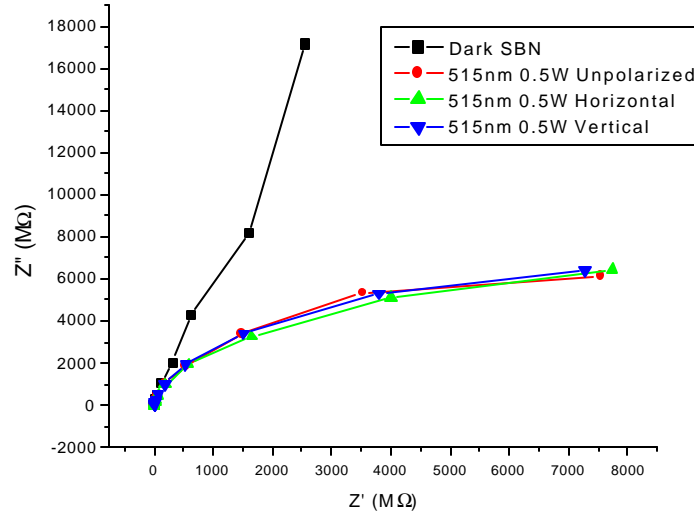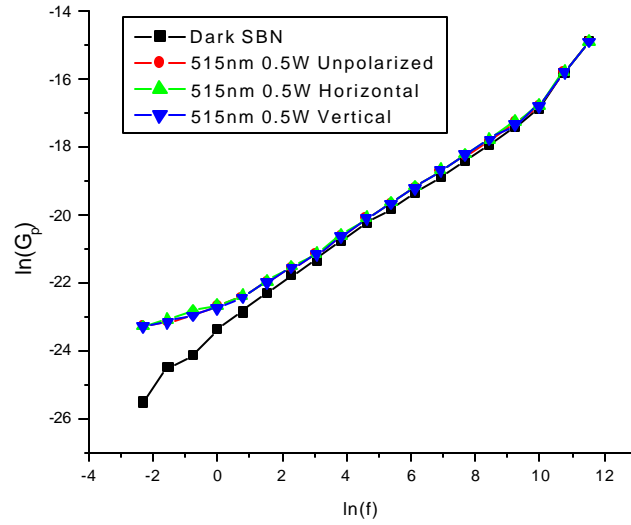
No significant polarization effects were observed. This was expected as the c-axis had been determined to be parallel to the propagation of the incident light.

VI. Conclusions

This study has shown that a.c. impedance spectroscopy is a useful tool in evaluating the electrical properties of SBN under optical stimulation. Ultraviolet, visible and infrared absorption measurements of a crystal sample of SBN revealed a band gap energy corresponding to a wavelength of approximately 390nm. In addition, the absorption data indicates that wavelengths associated with an Argon ion laser would be absorbed by the crystal, but would not exceed the bandgap energy. Significant inter-band energy states were evident in SBN from wavelengths of 390nm to longer than 500nm. Thus, the a.c. impedance investigation concentrated on the photoconductive behavior of SBN with optical stimulation over a wavelength range from 458nm to 515nm.

In the dark, this experiment showed that SBN is a very good insulator with very few conduction electrons. The primary electron transport mechanism is hopping as electrons move randomly from site to adjacent site without entering the conduction band. As illumination is introduced, SBN becomes less resistive and much more conductive. Electrons are excited out of states in the bandgap and into the conduction band. The main transport mechanism is no longer hopping: electrons are excited into the conduction band where they are mobile and consequently re-trapped into valence and inter-band energy states.

For SBN, the low frequency increase in conductance while under illumination is independent of the frequency of the applied voltage and increases linearly with applied optical power. At high applied electrical signal frequencies, however, this change in conductance becomes dependent on frequency and is no longer proportional to optical power.

When dark SBN is heated from room temperature to 70°C, the electron transport mechanism remains hopping. Despite a measurable decrease in impedance, it was shown that, within a range of incident power from 320 to 1930mW, optical excitation effects greatly overwhelm any thermal effects that may occur with optical absorption.

The photoconductivity of SBN was shown to be wavelength dependant in the blue-green from 458 to 515nm, with shorter wavelength, higher frequency radiation promoting a greater amount of charge to the conduction band. Polarization effects were not a factor in this crystal orientation, as the c-axis was parallel to the propagation of the incident light.

While this investigation shed much light on the electrical behavior and transport mechanism of photoconductive SBN, it also raised many new questions. In order to refine the results of this investigation and expand the electrical model of SBN, we intend to repeat the experiments detailed above on a sample of SBN doped with cerium to investigate the effects doping has on the transport mechanism. We also intend to investigate the effect of poling these samples, especially the effect on the dielectric constant. Finally, we hope to perform a series of experiments on partially illuminated SBN and compare those results with the fully illuminated impedance and dielectric data.

Appendix: Optical effects in SBN

A. Linear Electro-optic Effect

When SBN is illuminated bound charges from the crystal lattice are elevated to the conduction band. In a non-uniformly illuminated crystal of SBN, only electrons in the bright regions will have sufficient energy to jump across the band gap. These mobile electrons will drift, via diffusion, through the illuminated crystal lattice until they enter a dark region. Thus, electrons are trapped and "frozen," unable to move. This charge reorganization tends to set up a static electric field, known as a space-charge field, in the crystal, as a layer of negative charge is built up in the dark region and positive charge accumulates in the lighted areas. For a dielectric such as SBN, these static fields can have important consequences for the material's optical properties.

For a dielectric material, polarization depends on the applied electric field, the dielectric constant of the material and the susceptibility. This is written:

$$\vec{P} = \varepsilon_0 \chi \vec{E} \tag{A-1}$$

where the polarization is a vector determined by: ε_0, the permittivity of free space (a physical constant); χ, the dielectric's susceptibility to polarization; and $\vec{E}$, the electric field vector.

Light is an electromagnetic wave consisting of an electric field and a magnetic field propagating through space. For intense laser light, the magnitude of the electric field component can be large enough for the linear relationship of Eq. A-1 to break down. Taking this non-linear effect and expanding the magnitudes of A-1 as a power series gives:

$$P = e_0 (c^{(1)} E + c^{(2)} E^2 + c^{(3)} E^3 + ...) \tag{A-2}$$

where $\chi^{(1)}$ is the linear susceptibility in (1), and $\chi^{(2)}$, $\chi^{(3)}$,… are the non-linear susceptibilities.

SBN crystal structure lacks a quality known as inversion symmetry. In other words, there are directions within the crystal such that, if translation by $\vec{r}$ locates an atom, translation by $-\vec{r}$ will not. For example, if a body-centered cubic lattice has its center atom displaced slightly, the resulting structure lacks inversion symmetry. For crystals without inversion symmetry, the $\chi^{(2)}$ term will dominate the non-linear optical effects. Of the phenomena associated with $\chi^{(2)}$, the linear electro-optic effect deals with the effect of a small static field on the optical nature of the crystal.

If an electron in the crystal lattice can be assumed to be a small mass m of charge e on a spring that oscillates in one direction with a damping coefficient g and a resonant frequency ω_0, one can write the equation of motion:

$$m\ddot{x} + mk\dot{x} + m w_0{}^2 x + mq_2 x^2 = -e[E(w) + E_0] \tag{A-3}$$

where the left side of the equation consists of terms representing acceleration, damping, and a Hooke's law spring term. The fourth term is the quadratic correction due to $\chi^{(2)}$. The right side of the equation is the electrical force (remembering that $F = qE$) generated by the charge on the electron; the electric field component of light, $E(\omega)$; and the space-charge field, E_0, generated by the photoconductivity of SBN.

Assuming the quadratic correction to the spring force to be very small, it can be shown that the static field serves only to displace the electron. We can then write Eq. A-3 in terms of a new variable:

$$\boldsymbol{x} = x + eE_0 / m\boldsymbol{w}_0^2 \tag{A-4}$$

where x is the displacement of the electron.

In terms of Eq. A-4, the equation of motion becomes, after disregarding small terms proportional to E_0^2:

$$m\ddot{\boldsymbol{x}} + mk\dot{\boldsymbol{x}} + m(\boldsymbol{w}_0^2 - 2q_2 eE_0 / m\boldsymbol{w}_0^2)\boldsymbol{x} + mq_2\boldsymbol{x}^2 = -eE(\boldsymbol{w}) \tag{A-5}$$

Comparing Eq. A-5 to the equation of motion of the bound electron with no static field, it can be shown that the above relationship is the same, only with the resonant frequency shifted by an amount:

$$\Delta(\boldsymbol{w}_0^2) = 2q_2 eE_0 / m\boldsymbol{w}_0^2 \tag{A-6}$$

where $\Delta(\boldsymbol{w}_0^2)$ is the difference between the square of the resonant frequency and the frequency term in Eq. A-5.

The solution of the equation of motion for an electron that is unperturbed by a static field yields the following relationship for the index of refraction, a measure of the amount of interaction a material has with light (usually defined as the ratio of the speed of light in a vacuum to the speed of light in that material):

$$n^2 - 1 = (Ne^2 / m\boldsymbol{e}_0)(\boldsymbol{w}_0^2 - \boldsymbol{w}^2)^{-1} \tag{A-7}$$

where n is the index of refraction; N is the electron density of the material; m is the mass of one electron; e is the fundamental charge; ε_0 is the permittivity of free space; ω_0 is the resonant frequency of the electron; and ω is the frequency of the incident light[21].

Combining Eqs. A-6 and A-7 one can determine the effect this static field will have on the index of refraction:

$$\Delta n = \frac{q_2 e (n^2 - 1)}{m \mathbf{w}_0^2 (\mathbf{w}_0^2 - \mathbf{w}^2) n} E_0 \tag{A-8}$$

While this development has been simplified to only deal with one dimension, it is clear that a static field in a crystal that displays a large $\chi^{(2)}$ will change the index of refraction by a value that is linearly proportional to the field magnitude. Written in three dimensions, Eq. A-8 becomes:

$$\Delta n_{ijk} = -(n_{ijk}{}^3 r_{ijk}/2) E_0 \tag{A-9}$$

where r, the electro-optic coefficient, and n now depend on which axis of the crystal is affected. Nonetheless, the effect remains linearly proportional to the magnitude of the static field.[22]

B. Photorefractive Effect

This result has profound implications for ferroelectric crystals that display photoconductivity through a phenomenon known as the photorefractive effect. The creation of index gratings in the crystal through the electro-optic effect as the crystal is illuminated creates interesting optical reactions. Through photoconductivity, electrons

---

[21] T. S. Moss, et al, Semiconductor Opto-Electronics, (Wiley, New York, 1964), pp. 254-257.
[22] J. Feinberg, "Photorefractive Nonlinear Optics," *Physics Today*, October (1988) pp. 46-52.

are freed in the bright regions of these patterns and migrate to the dark. Static electric fields are set up between these areas of charge. Through the linear electro-optic effect, the index of refraction is changed in the regions affected by the space-charge fields. A material's index of refraction is a measure of how much light is affected in that medium. A light beam seems to bend, or refract, at an air-water interface because the index of refraction of water is higher than that of air. This means that the speed of light in water is less than the speed of light in air. A light beam striking water at some glancing angle will then bend toward the perpendicular as it travels through the water. A laser beam, encountering the many index variations "written" in SBN through the photorefractive effect, will be quite remarkably distorted.

In a common photorefractive effect, known as two-beam coupling, a poled photorefractive crystal is first illuminated uniformly by one beam, known as the reference beam, and then illuminated with a second tightly focused probe beam. In a few seconds, the probe beam will begin to gain power and the reference beam get weaker. Inside the crystal, through several complicated optical changes brought about by the index "gratings," the two beams have been coupled together and the probe beam robs the reference beam of much of its intensity.[23]

When laser light strikes poled SBN, it tends to scatter as it hits microscopic imperfections in the crystal. These scattered beams interfere constructively and destructively, creating microscopic interference patterns of dark and light regions in the bulk of the crystal and interact, through two-beam coupling, with the original incident beam. If a poled sample of a photorefractive crystal, such as SBN, is hit with a laser

---

[23] Feinberg, pp. 46-47.

beam, the light will first travel through the crystal unaffected. Gradually, however, as index variations are written and the scattered beams couple with the incident light, the beam exiting the crystal face will begin to spread out. After a few minutes, the exit beam will become a narrow fan of light as it spreads out, or diffracts, off of the many closely spaced, microscopic index variations formed in the crystal.

This index variation can be controlled, as well, producing several interesting applications of the photorefractive effect. One such possible application is the creation of wave-guides, or regions of the crystal that channel light waves in the same manner as fiber-optic cables. By controlling the size of the focused light beam that hits a poled photorefractive crystal in the presence of a strong external electric field, one can produce a semi-permanent index variation only in the small region that was illuminated by the laser. With a permanent region of higher refractive index, due to the linear electro-optic affect given in Eq. A-9 above, any light incident on this crystal will be channeled, by reflection and refraction, through this region with very small energy and power losses.

References

1. M. E. Lines and A. M. Glass, <u>Principles and Applications of Ferroelectrics and Related Materials</u>, (Clarendon, Oxford, 1987).

2. C. Kittel, <u>Introduction to Solid State Physics</u>, (Wiley, New York, 1986).

3. P. B. Jamieson, et al, "Ferroelectric Tungsten Bronze-Type Crystal Structures. I. Barium Strontium Niobate $Ba_{0.27}Sr_{0.75}Nb_2O_{5.78}$," The Journal of Chemical Physics **48**, 11 (1968).

4. J. R. Macdonald, <u>Impedance Spectroscopy: Emphasizing Solid Materials and Systems</u>, (Wiley, New York, 1985).

5. V. V. Daniel, <u>Dielectric Relaxation</u>, (Academic, London, 1967).

6. D. J. Griffiths, <u>Introduction to Electrodynamics</u>, 3rd ed., (Prentice, New Jersey, 1999).

7. G. R. Fowles, <u>Introduction to Modern Optics</u>, (Dover, New York, 1975).

8.   M. Pollak and T. H. Geballe, "Low-Frequency Conductivity Due to Hopping Processes in Silicon," Phys. Rev. **122**, 6 (1961).

9. M. Pollak, "Temperature Dependence of ac Hopping Conductivity," Phys. Rev. **138**, 6A (1965).

10. M. Pollack, "Approximations for the ac Impurity Hopping Conduction," Phys. Rev. **133**, 2A (1964).

11. M. Abkowitz, et al, "AC Conductivity and AC Photoconductivity in Amorphous and Crystalline Insulators," Phys. Rev. **9**, 4 (1974).

12. T. S. Moss, et al, <u>Semiconductor Opto-Electronics</u>, (Wiley, New York, 1964).

13. J. Feinberg, "Photorefractive Nonlinear Optics," Physics Today, October (1988).

MEMORANDUM

18 APR 2001

To: Prof. Shade
From: A. Prof. Steven Montgomery
        A. Prof. Charles Edmondson

SUBJ: TRIDENT REPORT FOR PETER BRERETON

1.   We have read this attached report and approve its submission to the Trident
        Committee.

                                        Respectfully,

                                        Steven R. Montgomery

                                        Charles A. Edmondson